

Old Dominion University
ODU Digital Commons

Physics Faculty Publications

Physics

2015

Fragmentation of Fast Josephson Vortices and Breakdown of Ordered States by Moving Topological Defects

Ahmad Sheikhzada

Alex Gurevich

Old Dominion University, agurevich@odu.edu

Follow this and additional works at: https://digitalcommons.odu.edu/physics_fac_pubs



Part of the [Physics Commons](#)

Repository Citation

Sheikhzada, Ahmad and Gurevich, Alex, "Fragmentation of Fast Josephson Vortices and Breakdown of Ordered States by Moving Topological Defects" (2015). *Physics Faculty Publications*. 48.

https://digitalcommons.odu.edu/physics_fac_pubs/48

Original Publication Citation

Sheikhzada, A., & Gurevich, A. (2015). Fragmentation of fast josephson vortices and breakdown of ordered states by moving topological defects. *Scientific Reports*, 5,17821. doi: 10.1038/srep17821

SCIENTIFIC REPORTS



OPEN

Fragmentation of Fast Josephson Vortices and Breakdown of Ordered States by Moving Topological Defects

Received: 25 September 2015

Accepted: 06 November 2015

Published: 07 December 2015

Ahmad Sheikhzada & Alex Gurevich

Topological defects such as vortices, dislocations or domain walls define many important effects in superconductivity, superfluidity, magnetism, liquid crystals, and plasticity of solids. Here we address the breakdown of the topologically-protected stability of such defects driven by strong external forces. We focus on Josephson vortices that appear at planar weak links of suppressed superconductivity which have attracted much attention for electronic applications, new sources of THz radiation, and low-dissipative computing. Our numerical simulations show that a rapidly moving vortex driven by a constant current becomes unstable with respect to generation of vortex-antivortex pairs caused by Cherenkov radiation. As a result, vortices and antivortices become spatially separated and accumulate continuously on the opposite sides of an expanding dissipative domain. This effect is most pronounced in thin film edge Josephson junctions at low temperatures where a single vortex can switch the whole junction into a resistive state at currents well below the Josephson critical current. Our work gives a new insight into instability of a moving topological defect which destroys global long-range order in a way that is remarkably similar to the crack propagation in solids.

Quantized vortex lines are quintessential topological defects^{1,2} which determine the behavior of superconductors and superfluids. Vortices in superconductors are characterized by an integer winding number n in the phase φ of the complex order parameter $\Psi = \Delta \exp(i\varphi)$, singularity of $\nabla\varphi$ in a vortex core, and the quantized magnetic flux, $\phi = n\phi_0$, where $\phi_0 = h/2e = 2.07 \times 10^{-15}$ Wb is the magnetic flux quantum, e is the electron charge and h is the Planck constant. Because destruction of a topological defect requires overcoming a huge energy barrier proportional to the length or the area of a system, vortices can only disappear by annihilating with antivortices with the opposite sign of n or exiting through the sample surface, or forming shrinking loops. This brings about the question: does this fundamental, topologically-protected stability of vortices remain preserved for a vortex driven by a strong force and, more generally, what happens to a global long-range order if a moving topological defect becomes unstable? To address this issue, we performed numerical simulations of vortices in superconducting-insulating-superconducting (SIS) Josephson junctions^{3,4} where the lack of suppression of the superconducting gap $\Delta(r)$ greatly reduces viscous drag of vortices, allowing them to reach velocities as high as a few percent of the speed of light c under a strong current drive. Dynamics of superfast Josephson vortices has been probed in annular thin film junctions⁵, and has recently attracted much attention for the development of superconducting qubits and low-dissipative digital memory⁶⁻⁸, and new sources of THz radiation⁹. We show that a rapidly moving vortex can become unstable, causing a cascade of expanding vortex-antivortex pairs, which eventually destroy the global long-range order. This effect may impose limitations on the performance of Josephson memory⁶⁻⁸, superconducting sources of

Department of Physics and the Center for Accelerator Science, Old Dominion University, Norfolk, VA 23529, USA. Correspondence and requests for materials should be addressed to A.S. (email: ashei003@odu.edu) or A.G. (email: gurevich@odu.edu)

THz radiation⁹, or polycrystalline superconducting resonator cavities for particle accelerators¹⁰, and have broader implications for other systems with long-range order.

We start with a standard theory of a Josephson vortex in a long junction described by the sine-Gordon equation for the phase difference of the order parameter $\theta(x, t) = \varphi_1 - \varphi_2$ between two bulk electrodes^{3,4}:

$$\ddot{\theta} + \eta\dot{\theta} = \theta'' - \sin\theta + \beta. \quad (1)$$

Here the prime and the overdot denote partial derivatives with respect to the dimensionless coordinate x/λ_J and time $\omega_J t$, $\omega_J = (2\pi J_c/\phi_0 C)^{1/2}$ is the Josephson plasma frequency, J_c is the tunneling critical current density, C is the specific capacitance of the junction, $\lambda_J = (\phi_0/4\pi\mu_0\lambda J_c)^{1/2}$ is the Josephson penetration depth, λ is the London penetration depth, $\eta = 1/\omega_J RC$ is the damping constant due to the ohmic quasiparticle resistance R , and $\beta = JJ_c$ is the driving parameter controlled by a uniform transport current density J .

The sine-Gordon equation has been one of the most widely used equations to describe topological defects in charge and spin density waves¹¹, commensurate-incommensurate transitions^{12–14}, magnetic domain walls¹⁵, dislocations in crystals^{16,17}, kinks on DNA molecules^{18,19}, etc. Particularly, the 2π kink solution $\theta(x, t) = 4 \tan^{-1} \exp[(x - vt)/L]$ of equation (1) at $\eta \rightarrow 0$ describes a Josephson vortex of width $L = (1 - v^2/c_s^2)^{1/2} \lambda_J$ moving with a constant velocity v , where $c_s = \omega_J \lambda_J$ is the Swihart velocity of propagation of electromagnetic waves along the junction³. As v increases, the vortex shrinks at $\eta \ll 1$ and expands at $\eta > 1$ ⁴.

The Lorentz-like contraction of the Josephson vortex at $\eta \ll 1$ indicates that equation (1) should be modified at large velocities if $L(v)$ approaches the geometry-dependent magnetic screening length Λ . Indeed, equation (1) was obtained assuming that both $\theta(x, t)$ and the magnetic field $B(x, t)$ produced by vortex currents vary slowly along the junction over the same length $\sim L(v) \gg \Lambda$ ³; otherwise $\theta(x, t)$ and $B(x, t)$ vary over *different* lengths and the relation between $B(x, t)$ and $\theta(x, t)$ becomes nonlocal⁴. The equation, which generalizes equation (1) to $\theta(x, t)$ and $B(x, t)$ varying over any lengths larger than the superconducting coherence length ξ , is given by^{20–23}:

$$\ddot{\theta} + \eta\dot{\theta} = \epsilon \int_{-\infty}^{\infty} G\left(\frac{|x-u|}{\alpha}\right) \frac{\partial^2 \theta}{\partial u^2} du - \sin\theta + \beta, \quad (2)$$

where $\epsilon = \lambda_J/\lambda$, $\alpha = \Lambda/\lambda_J$, and the kernel $G(x)$ depends on the sample geometry. Here $G(x/\alpha) = \pi^{-1} K_0(x/\alpha)$ for a planar junction in a bulk superconductor, where $\alpha = \lambda/\lambda_J$ and $K_0(x)$ is the modified Bessel function²¹. For an edge junction in a thin film of thickness $t \ll \lambda$, we have $2G(x/\alpha) = \mathbf{H}_0(x/\alpha) - Y_0(x/\alpha)$, where $\alpha = 2\lambda^2/t\lambda_J$, and $\mathbf{H}_0(x)$ and $Y_0(x)$ are the Struve and Bessel functions, respectively^{22,23}. The kernels $G(x, u)$ for different geometries decrease with u at $|x-u| > \Lambda$ and have the same logarithmic singularity at $u = x$ ^{20–23}. The nonlocal effects are most pronounced at $\lambda_J^2/\lambda < \Lambda$, particularly in high- J_c bulk junctions with $J_c > J_d/\kappa$ ²¹ and thin film junctions^{20,22–24} with large Pearl length $\Lambda = 2\lambda^2/t$, where $J_d = \phi_0/2^{3/2}\mu_0\lambda^2\xi$ is the depairing current density, and $\kappa = \lambda/\xi$. At $\lambda_J^2/\lambda \ll \Lambda$, only the universal logarithmic part of $G(x, u)$

$$G_0(|x-u|/\alpha) = \pi^{-1} \ln(\alpha/|x-u|) \quad (3)$$

is essential, while a nonsingular, geometry-dependent part of $G(x, u)$ can be disregarded^{21–23}. Equations (2)–(3) describe mixed Abrikosov vortices with Josephson cores of length $l = \lambda_J^2/\lambda \simeq \xi J_d/J_c$ along the junction (AJ vortices)²¹. Equations (2)–(3) in the overdamped limit of $\eta \gg 1$ have an exact solution $\theta(x, t) = \pi + \sin^{-1} \beta + 2 \tan^{-1}[(x - vt)/L]$ that describes a driven AJ vortex core with weak suppression of $\Delta(x)$ and the length $L = (1 - \beta^2)^{-1/2} l$ expanding as β increases²¹. AJ vortices have been observed in flux flow experiments on low-angle grain boundaries of high- T_c cuprates²⁵, the c -axes resistivity in layered pnictides²⁶, and most recently by STM imaging of step edge junctions in Pb and In monolayers on Si substrates^{27,28}. Equations (2)–(3) also reduce to the Peierls equation that describes slow dislocations in crystals¹⁶.

Unlike the sine-Gordon equation, the nonlocal equation (2) at $\eta = 0$ is not Lorentz-invariant, so a uniformly moving vortex can radiate Cherenkov waves $\delta\theta(x, t) \propto \exp(ikx - i\omega_k t)$ with the phase velocities ω_k/k smaller than v ^{23,29}. The condition of Cherenkov radiation at $\eta = 0$ is given by:

$$kv > \omega_J \left[\sqrt{1 - \beta^2} + lk^2 G(k) \right]^{1/2}, \quad (4)$$

where $l = \lambda_J^2/\lambda = \phi_0/4\pi\mu_0\lambda^2 J_c$, and $G(k)$ is the Fourier image of $G(x)$. Here $G(k)$ decreases as $1/k$ at $k > \Lambda^{-1}$ so equation (4) is satisfied for $k > k_c$ where the maximum wavelength $2\pi/k_c$ increases with v ³⁰. To address the effect of Cherenkov radiation on the moving vortex, we performed numerical simulations of equation (2) for SIS junctions of different geometries.

Shown in Fig. 1 are the numerical results for a planar bulk junction at $\eta = 0.05$ and the large ratio $\lambda_J/\lambda = 10$ usually described by the sine-Gordon equation (1). Yet the more general integral equation (2) reveals the effects which are not captured by equation (1), particularly a trailing tail of Cherenkov

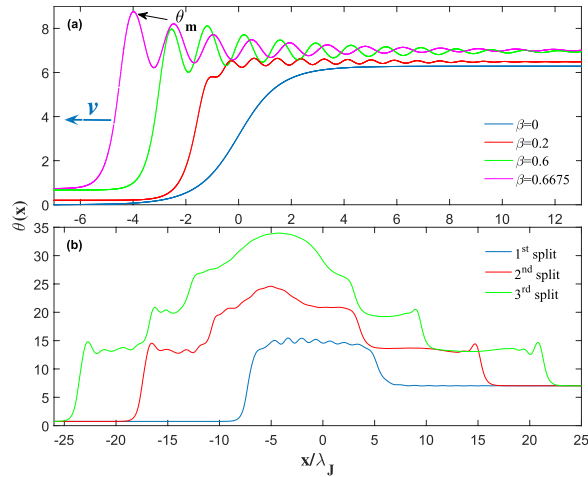


Figure 1. Steady-state vortex profiles and the initial stage of fragmentation instability. (a) A sequence of phase profiles in a propagating vortex (shifted horizontally for clarity in the moving frames) calculated for a bulk junction by solving equation (2) for different values of β , $\eta = 0.05$, and $\lambda_J/\lambda = 10$. At $\beta_s = 0.6676$ the peak amplitude of Cherenkov wave reaches $\theta_c = 8.76$ and starts growing and evolving into an expanding vortex-antivortex pair. (b) Snapshots of $\theta(x)$ at $\beta = \beta_s$ which show first three dissociations of the unstable vortex into vortex-antivortex pairs accompanied by Cherenkov radiation. Movies showing the initial stage of vortex instability and formation of the phase pile after multiple generations of vortex-antivortex pairs are available in ref. 30. Notice that $\theta(\infty) - \theta(-\infty) = 2\pi$ remains fixed by the phase difference in the initial vortex.

radiation behind a vortex moving with a constant velocity²⁹. Moreover, as the amplitude and the wavelength of radiation increase with v , the vortex becomes unstable at $\beta > \beta_s$, the instability is triggered at the highest maximum of Cherenkov wave where θ_m reaches a critical value $\theta_c \approx 8.65\text{--}8.84$, depending on η , λ/Λ , and the junction geometry³⁰. Here θ_c is confined within the interval $5\pi/2 < \theta_c < 3\pi$ in which a uniform state of a Josephson junction is unstable^{3,4}. As the velocity increases, the domain where $5\pi/2 < \theta(x - vt) < 3\pi$ behind the moving vortex widens and eventually becomes unstable as its length exceeds a critical value. This suggests a qualitative picture of the vortex instability caused by the appearance of a trailing critical nucleus being in the unstable π -junction state^{3,4} caused by strong Cherenkov radiation. The latter appears entirely due to the Josephson nonlocality described by equation (2), which has no steady-state vortex solutions at $J > J_s$ where J_s can be well below J_c at which the whole junction switches into a resistive state.

The dynamic solutions of equation (2) at $\beta > \beta_s$ change strikingly. Our simulations have shown that the instability originates at the highest maximum $\theta = \theta_m$ of the trailing Cherenkov wave which starts growing and eventually turning into an expanding vortex-antivortex pair³⁰, as shown in Fig. 1. As the size of this pair grows, it generates enough Cherenkov radiation to produce two more vortex-antivortex pairs which in turn produce new pairs. Continuous generation of vortex-antivortex pairs results in an expanding dissipative domain in which vortices accumulate at the left side, antivortices accumulate at the right side, while dissociated vortices and antivortices pass through each other in the middle³⁰. As a result, $\theta(x, t)$ evolves into a growing “phase pile” with the maximum $\theta_m(t)$ increasing approximately linear with time and the edges propagating with a speed which can be both smaller and larger than c_s , the phase difference $\theta(\infty) - \theta(-\infty) = 2\pi$ between the edges remains fixed. We observed the phase pile dynamic state for different junction geometries and η ranging from 10^{-3} to 0.5 ³⁰. For instance, Figs 2 and 3 show the 3D images of the initial stage of dynamic separation of vortices and antivortices calculated for a bulk junction and a thin-film edge junction. Here the local magnetic field $B(x, t)$ oscillates strongly at the moving domain edges but becomes rather smooth away from them, as shown in Fig. 4. In the most part of the phase pile overlapping vortices are indistinguishable, yet the net flux $\phi = \phi_0$ of this evolving multi-quanta magnetic dipole remains quantized.

Shown in Fig. 5 are the steady-state vortex velocities $v(\beta)$ calculated for different junction geometries. The instability corresponds to the endpoints of the $v(\beta)$ curves which have two distinct parts. At small $\beta \lesssim \eta$ the velocity $v(\beta)$ increases sharply with a slope limited by a weak quasiparticle viscous drag. At larger $\beta \gtrsim \eta$ the increase of $v(\beta)$ with β slows down, as the vortex velocities are mostly limited by radiation friction²⁹ and depend weakly on the form of dissipative terms in equation (2). For a low- J_c junction with $\lambda_J/\lambda = 10$, the effect of Cherenkov radiation on $v(\beta)$ is weak, but for a high- J_c bulk junction with $\lambda/\lambda_J = \sqrt{10}$ and $\eta \ll 1$, radiation friction dominates at practically all β , significantly reducing both $v(\beta)$ and β_s .

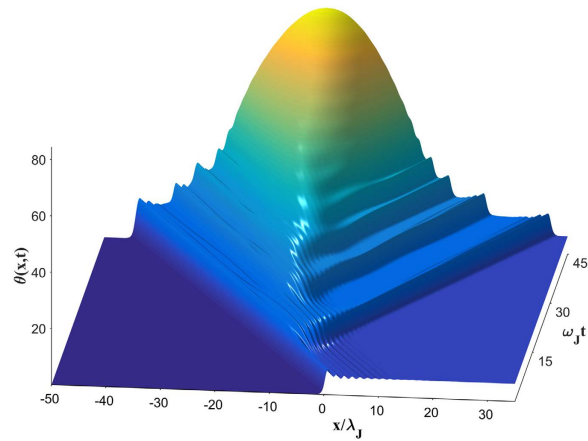


Figure 2. A 3D image of the evolution of phase pile triggered by an unstable vortex. The dynamic phase distribution $\theta(x, t)$ was calculated from equation (2) for a bulk junction at $\beta = 0.6676$, $\lambda_j/\lambda = 10$ and $\eta = 0.05$. Here the maximum phase $\theta_m(t)$ increases approximately linearly with time while the edge vortices move with constant velocities close to c_s . Individual vortices and antivortices clearly visible at the edges of the expanding phase pile overlap strongly toward its central part.

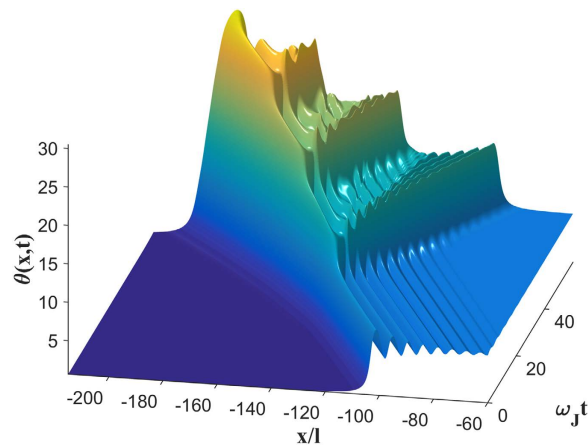


Figure 3. A 3D image of vortex instability and the initial stage of the phase pile formation in nonlocal regime. The dynamic phase distribution was calculated at $\beta = \beta_s = 0.63$ for a thin film edge junction with $\eta = 0.1$ and $l = \Lambda/2$. Here $\theta(x, t)$ in the vortex at $\beta = \beta_s$ was computed by solving the full dynamic equation (2) with the initial distribution equal to the stable single-vortex solution $\theta(x - vt)$ calculated at $\beta = \beta_s - 0.01$. As a result, the vortex then accelerates slightly and becomes unstable, triggering the growth of the phase pile. After multiple generations of vortex-antivortex pairs, vortices at the leading edges reach velocities of $1.12l\omega_j$.

For thin film edge junctions, the critical splitting current density J_s gets reduced down to $J_s \approx 0.4J_c$ at $\eta = 10^{-3}$, as shown in Fig. 5. In the extreme nonlocal limit described by equations (2) and (3), the maximum velocity $v_s = v(J_s)$ at which the steady-state moving vortex remains stable, can be written in the scaling form $v_s = c_s \lambda_j f(\eta)/\lambda$, where $f(\eta)$ decreases from ≈ 2.5 at $\eta = 0.5$ to ≈ 1 at $\eta = 10^{-3}$. The Josephson vortex in thin film edge junctions can reach the velocities exceeding the nominal Swihart velocity $c_s = \omega_j \lambda_j$ at $J \approx J_s$ if $\lambda_j > \lambda$ but $l < \Lambda$, that is, $t < 2\lambda^3/\lambda_j^2$. Dynamics of $\theta(x, t)$ in the nonlocal limit at $J > J_s$ is similar to that is shown in Figs 1–3, except that the edges of phase pile can propagate with “superluminal” velocities $v \approx v_s > c_s$ if $\lambda_j > \lambda^{30}$. Once vortex-antivortex pairs start replicating, the speed of leading vortices at the edges gradually increases from v_s to a limiting value v_∞ , for instance, from $v_s \approx 0.72l\omega_j$ to $v_\infty \approx 1.12l\omega_j$ for an edge junction with $l = \Lambda/2$ and $\eta = 0.1^{30}$.

The effects reported here are most pronounced in underdamped SIS junctions between s-wave superconductors at low temperatures for which the viscous drag coefficient $\eta \propto \exp(-\Delta/T)$ due to thermally-activated quasiparticles³ is small. Here $\eta \ll 1$ also implies that a moving vortex does not generate additional quasiparticles because the induced Josephson voltage $V = v\hbar\theta'_m/2eL$ is smaller than Δ/e , where θ'_m is the maximum phase gradient. These conditions are satisfied for the parameters used in

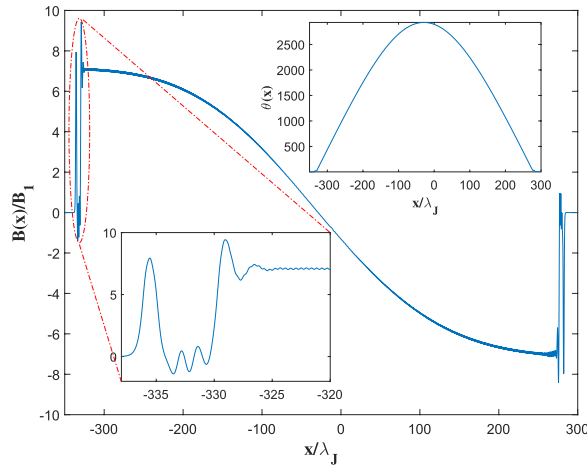


Figure 4. A snapshot of the normalized magnetic field $B(x, t)/B_1$. Here $B(x, t)$ was calculated from equation (2) for a bulk junction at $\eta = 0.05$, $\beta = 0.6676$, $\lambda_J/\lambda = 10$ and $B_1 = \phi_0/2\pi\lambda\lambda_J$. Inset shows the corresponding phase distribution, $\theta(x, t)$. One can clearly see a complex structure of the left leading edge comprised of a vortex overlapping with a vortex-antivortex pair. Away from the edges vortices overlap so strongly that the Cherenkov radiation gets suppressed almost to zero, and the smooth distribution of $B(x, t)$ in the growing resistive domain can be regarded as a giant multiquanta vortex-antivortex dipole.

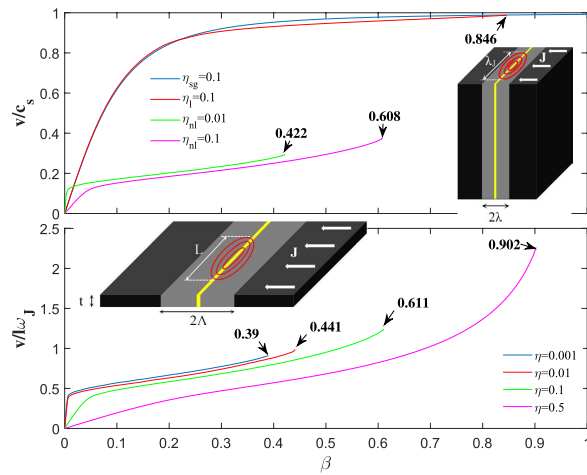


Figure 5. Velocities of a stable single vortex $v(\beta)$ as functions of current calculated for different junction geometries. The instability occurs at the endpoints (shown by arrows) of the $v(\beta)$ curves. The upper panel shows $v(\beta)$ for a bulk junction calculated from equation (2) at $\eta_l = 0.1$ in the seemingly conventional weak-link limit, $\lambda_J/\lambda = 10$ (for comparison, the blue curve shows $v(\beta)$ calculated from eq. (1) at $\eta_{sg} = 0.1$). The magenta and green curves show $v(\beta)$ calculated for a bulk nonlocal junction with $\lambda/\lambda_J = \sqrt{10}$ for values of $\eta_{nl} = 0.1$ and $\eta_{nl} = 0.01$, respectively, where the indices *sg*, *l* and *nl* correspond to the pure sine-Gordon, weakly nonlocal and strongly nonlocal limits, respectively. The lower panel shows results for a thin film edge junction in the extreme nonlocal limit described by equations (2) and (3). Notice that both the $v(\beta)$ curves and the critical values β_c at $\eta = 0.1$ and $\eta = 0.01$ for the thin film junction are close to those for the bulk junction shown in the upper panel. This is because for a nonlocal bulk junction, $\theta'(u)$ in equation (2) has a sharp peak of width $\sim(\lambda_J/\lambda)^2\lambda = 0.1\lambda$ so $G[(x-u)/\alpha] = \pi^{-1}K_0[|x-u|/\alpha]$ can be approximated by its expansion at small argument, $K_0(x/\alpha) \rightarrow \ln(2\alpha/|x|) - 0.577$, which reduces to equation (3). Here any constant factor under the log does not affect $\theta(x, t)$ since $\theta'(-\infty) = \theta'(\infty) = 0$.

the calculations and are facilitated by the electromagnetic nonlocality of thin film edge junctions³⁰, particularly monolayer junctions^{27,28}. Furthermore, a small power P dissipated by a moving vortex at $\eta \ll 1$ does not really affect the Cherenkov instability. For instance, P generated by a vortex at the critical velocity $v_s \simeq \omega_J l$ in a thin film junction is given by³⁰:

$$P \simeq \frac{\phi_0^2 t}{4\pi\mu_0\lambda^2 RC} \quad (5)$$

This equation shows that the power P is independent of J_c and is greatly reduced in the underdamped limit at low temperatures as the quasiparticle resistance R of SIS junctions becomes exponentially large at $T \ll T_c$. To estimate P , it is convenient to write equation (5) in the form $P \simeq \eta\varepsilon_0 t\omega_j$, where $\varepsilon_0 = \phi_0^2/4\pi\mu_0\lambda^2$ is a characteristic line energy of Abrikosov vortex³¹. For an edge junction in a Nb film with $t = 1$ nm, $\lambda = 40$ nm, $\varepsilon_0 \sim 10^4$ kelvin/nm, and $\omega_j = 100$ GHz much smaller than $\Delta/\hbar \simeq 2.4$ THz¹⁰, equation (5) yields $P \sim 0.16$ nW at $\eta = 10^{-2}$. Local overheating $\delta T = PY_K$ caused by vortex dissipation is further reduced in thin film junctions for which the energy transfer to the substrate due to ballistic phonons is much more effective than diffusive phonon heat transport in thick samples, where Y_K is the Kapitza interface thermal resistance³². Such weak overheating caused by a moving vortex cannot result in thermal bistability and hysteric switching due to hotspot formation³².

Proliferation of vortex-antivortex pairs triggered by a moving Josephson vortex can be essential for the physics and applications of weak link superconducting structures where the formation of expanding phase pile patterns can switch the entire junction into a normal state at currents well below the Josephson critical current, $J > J_s \simeq (0.4-0.7)J_c$. Such dynamic vortex instability can result in hysteretic jumps on the V-I curves which appear similar to those produced by heating effects^{4,9}, yet this instability is affected by neither cooling conditions nor the nonequilibrium kinetics of quasiparticles. Indeed, heating is most pronounced in overdamped junctions with $\eta > 1$ in which Cherenkov radiation is suppressed. By contrast, the Cherenkov instability is characteristic of the weakly-dissipative underdamped limit $\eta \ll 1$, although Fig. 5 shows that this instability in thin film edge junctions can persist up to $\eta = 0.5$. Therefore, the crucial initial stage of the phase pile formation at $\eta \ll 1$ is unaffected by heating which may become more essential at the final stages of the transition of the entire junction into the normal state. At $\eta \sim 1$ the Cherenkov instability may be masked by heating effects, particularly in bulk junctions for which heat transfer to the coolant is less efficient than in thin films.

It should be emphasized that the instability reported here does not require special junctions with $J_c \sim J_d$. In fact, even for the seemingly conventional bulk junction with $\lambda_j = 10\lambda$ shown on the top panel of Fig. 5, the instability at $J_s \simeq 0.846J_c$ implies $J_c \sim 0.01J_d/\kappa$, which translates into $J_c \sim 10^{-4}J_d$ for bulk NbN junctions. Moreover, in wide thin film edge junctions the nonlocality becomes important at even much lower J_c , as is evident from the lower panel of Fig. 5. Therefore, the effects reported here can occur in conventional underdamped junctions with $J_c \ll J_d$, particularly wide thin film or monolayer edge junctions. Interaction of Josephson vortices with pinned Abrikosov vortices in electrodes can result in additional mechanisms of splitting instability of Josephson vortices. For instance, radiation by Josephson vortices can be greatly enhanced as they move in a periodic magnetic potential of Abrikosov vortices along weak link grain boundaries^{25,33}, whereas Abrikosov vortices trapped perpendicular to the Josephson junction can result in generation of Josephson vortex-antivortex pairs in the presence of the applied electric current³⁴.

Our results can be essential for other topological defects such as crystal dislocations or magnetic domain walls described by the generic nonlocal equation (2) in which the integral term results from a common procedure of reduction of coupled evolution equations for several relevant fields to a single equation. For Josephson junctions, such coupled fields are θ and B , but for domain walls in ferromagnets, the nonlocality can result from long-range magnetic dipolar interactions³⁵. For dislocations, the nonlocality and Cherenkov radiation of sound waves in equation (2) come from the discreteness of the crystal lattice¹⁷ and long-range strain fields¹⁶, although the dynamic terms in the Peierls equation^{36,37} are more complex than those in equation (2). Dynamic instabilities of dislocations have been observed in the lattice Frenkel-Kontorova models¹⁷ in which sonic radiation can also result from periodic acceleration and deceleration of a dislocation moving in a crystal Peierls-Nabarro potential¹⁶. The latter effect becomes more pronounced as the dislocation core shrinks at higher velocities and becomes pinned more effectively by the lattice. By contrast, the instability reported here results entirely from Cherenkov radiation, the condition (4) can be satisfied for any system in which $G(k)$ in equation (4) decreases with k . This instability can thus have broader implications: for instance, the phase pile dynamics of Josephson vortices appears similar to a microcrack propagation caused by a continuous pileup of subsonic dislocations with antiparallel Burgers vectors at the opposite tips of a growing crack described by equations (2) and (3)¹⁶.

Our results give a new insight into breakdown of a global long-range order which has been usually associated with either thermally-activated proliferation of topological defects (like in the Berezinskii-Kosterlitz-Thouless transition) or static arrays of quenched topological defects pinned by the materials disorder². Here we point out a different mechanism in which a long-range order is destroyed as a single topological defect driven by a strong external force becomes unstable and triggers a cascade of expanding pairs of topological defects of opposite polarity.

Methods

We have developed an efficient MATLAB numerical code to solve the main integro-differential equation (2) using the method of lines³⁸. By discretizing the integral term in equation (2) it was reduced to a set

of coupled nonlinear ordinary differential equations in time which were solved by the multistep, variable order Adams-Bashforth-Moulton method³⁹. We have checked our numerical results using a slower iterative method to make sure that the logarithmic singularity of $G(x-u)$ is handled properly, the absolute and relative error tolerances were kept below 10^{-6} . The length L_b of computational box $x_1 < x < x_1 + L_b$ along the x -axis (either co-moving with the vortex or expanding with the phase pile) was taken large enough to assure no artifacts coming from possible reflected waves at $x = x_1$ and $x = x_1 + L_b$. We set $\theta(x_1, t) - \sin^{-1}\beta < 10^{-6}$ and $\theta(x_1 + L_b, t) - 2\pi - \sin^{-1}\beta < 10^{-6}$ and made sure that changing L_b does not affect the results, where L_b was typically taken at least three times larger than the spatial extent of $\theta(x, t)$, be it a single vortex or expanding phase pile. The steady state phase distribution $\theta(x-vt)$ in a uniformly moving vortex at a given β was computed by solving the full dynamic equation (2) using the single-vortex solution calculated at a smaller preceding value of β as an initial condition. The code then run until the velocity of the vortex stabilizes to the accuracy better than 0.1%.

References

1. N. D. Mermin. The topological theory of defects in ordered media. *Rev. Mod. Phys.* **51**, 591–648 (1979).
2. Chaikin, P. M. & Lubensky, T. C. *Principles of Condensed Matter Physics*. (Cambridge University Press, Cambridge, New York, Madrid, 2010).
3. Barone, A. & Paterno, G. *Physics and Applications of Josephson Effects* (Wiley, New York, 1982).
4. Likharev, K. K. *Dynamics of Josephson Junctions and Circuits* (Gordon and Breach Science Publishers, New York, 1986).
5. Ustinov, A. V. *et al.* Dynamics of sine-Gordon solitons in the annular Josephson junction. *Phys. Rev. Lett.* **69**, 1815–1818 (1992).
6. Herr, A., Fedorov, A., Shnirman, A., Il'ichev, E. & Schon, G. Design of a ballistic fluxon qubit readout. *Supercond. Sci. Technol.* **20**, S450 (2007).
7. Devoret, M. & Schoelkopf, R. Superconducting circuits for quantum information: An outlook. *Science* **339**, 1169–1174 (2013).
8. Fedorov, K. G., Shcherbakova, A. V., Wolf, M. J., Beckmann, D. & Ustinov, A. V. Fluxon readout of a superconducting qubit. *Phys. Rev. Lett.* **112**, 160502 (2014).
9. Welp, U., Kadowaki, K. & Kleiner, R. Superconducting emitters of THz radiation. *Nature Photonics* **7**, 702–710 (2013).
10. Gurevich, A. Superconductivity radio-frequency fundamentals for particle accelerators. *Rev. Accel. Sci. Technol.* **5**, 119–146 (2012).
11. Grüner, G. The dynamics of charge density waves. *Rev. Mod. Phys.* **60**, 1129–1181 (1988).
12. Pokrovsky, V. L. & Talapov, A. L. Ground state, spectrum, and phase diagram of 2-dimensional incommensurate crystals. *Phys. Rev. Lett.* **42**, 65–67 (1979).
13. Bak, P. Commensurate phases, incommensurate phases, and devil's staircase. *Rep. Prog. Phys.* **45**, 587–629 (1982).
14. Woods, C. R. *et al.* Commensurate-incommensurate transition in graphene on hexagonal boron nitride. *Nature Phys.* **10**, 451–456 (2014).
15. Bar'yakhtar, V. G., Chetkin, M. V., Ivanov, B. A. & Gadetskii, S. N. *Dynamics of Topological Magnetic Solitons*. (Springer-Verlag, Berlin, Heidelberg, New York, 1994).
16. Hirth, J. B. & Lothe, J. *Theory of Dislocations*. (McGraw-Hill, New York, 1968).
17. Braun, O. M. & Kivshar, Yu. S. *The Frenkel-Kontorova Model: Concepts, Methods, and Applications* (Springer-Verlag, Berlin, New York, 2004).
18. Salerno, M. Discrete model for DNA-promoter dynamics. *Phys. Rev. A* **44**, 5292–5297 (1991).
19. Yakushevich, L. V. *Nonlinear physics of DNA* (2nd ed., John Wiley and Sons, 2006).
20. Ivanchenko, Yu. M. & Sobleva, T. K. Nonlocal interaction in Josephson junctions. *Phys. Lett. A* **147**, 65–69 (1990).
21. Gurevich, A. Nonlinear viscous motion of vortices in Josephson contacts. *Phys. Rev. B* **48**, 12857–12865 (1993).
22. Kogan, V. G., Dobrovitski, V. V., Clem, J. R., Mawatari, Y. & Mints, R. G. Josephson junction in a thin film. *Phys. Rev. B* **63**, 144501 (2001).
23. Abdulmalikov, A. A., Alfimov, G. L. & Malishevskii, A. S. Nonlocal electrostatics of Josephson vortices in superconducting circuits. *Supercond. Sci. Technol.* **22** 023001 (2009).
24. Boris, A. A. *et al.* Evidence for nonlocal electrostatics in planar Josephson junctions. *Phys. Rev. Lett.* **111**, 117002 (2013).
25. Gurevich, A. *et al.* Flux flow of Abrikosov-Josephson vortices along grain boundaries in high-temperature superconductors. *Phys. Rev. Lett.* **88**, 097001 (2002).
26. Moll, P. J. W. *et al.* Transition from slow Abrikosov to fast moving Josephson vortices in iron pnictide superconductors. *Nature Mater.* **12**, 134–138 (2013).
27. Brun, C. *et al.* Remarkable effects of disorder on superconductivity of single atomic layers of lead on silicon. *Nature Phys.* **10**, 444–450 (2014).
28. Yoshizawa, S. *et al.* Imaging Josephson vortices on the surface superconductor Si (111)-($\sqrt{7} \times \sqrt{3}$)-In using a scanning tunneling microscope. *Phys. Rev. Lett.* **113**, 247004 (2014).
29. Mints, R. G. & Snapiro, I. B. Josephson-vortex Cherenkov radiation. *Phys. Rev. B* **52** 9691 (1995).
30. See the Supplemental Information for details of calculations and movies of vortex instabilities for different junction geometries.
31. Blatter, G., Feigel'man, M. V., Geshkenbein, V. B., Larkin, A. I. & Vinokur, V. M. Vortices in high-temperature superconductors. *Rev. Mod. Phys.* **66**, 1125–1532 (1994).
32. Gurevich, A. V. & Mints, R. G. Self-heating in normal metals and superconductors. *Rev. Mod. Phys.* **59**, 941–999 (1987).
33. Gurevich, A. & Cooley, L. D. Anisotropic flux pinning in a network of planar defects. *Phys. Rev. B* **50**, 13563–13576 (1994).
34. Berdiyrov, G. R., Milosević, M. V., Savelev, S., Kusmartsev, F. & Peeters, F. M. Parametric amplification of vortex-antivortex pair generation in a Josephson junction. *Phys. Rev. B* **90**, 134505 (2014).
35. Cizeau, P., Zapperi, S., Durin, G. & Stanley, H. E. Dynamics of a ferromagnetic domain wall and the Barkhausen effect. *Phys. Rev. Lett.* **79**, 4669–4672 (1997).
36. Rosakis, P. Supersonic dislocation kinetics from an augmented Peierls model. *Phys. Rev. Lett.* **86**, 95–98 (2001).
37. Pillon, L., Denoual, C. & Pellegrini, Y. P. Equation of motion for dislocations with inertial effects. *Phys. Rev. B* **76**, 224105 (2007).
38. Schiesser, W. E. *The Numerical Method of Lines: Integration of Partial Differential Equations* (Academic Press, San Diego, 1991).
39. Shampine, L. F. & Gordon, M. K. *Computer Solution of Ordinary Differential Equations: The Initial Value Problem* (W. H. Freeman, San Francisco, 1975).

Acknowledgements

This work was supported by the United States Department of Energy under Grant No. DE-SC0010081.

Author Contributions

A.S. performed all numerical simulations described here, and A.G. directed the project. Both authors contributed to the manuscript.

Additional Information

Supplementary information accompanies this paper at <http://www.nature.com/srep>

Competing financial interests: The authors declare no competing financial interests.

How to cite this article: Sheikhzada, A. and Gurevich, A. Fragmentation of Fast Josephson Vortices and Breakdown of Ordered States by Moving Topological Defects. *Sci. Rep.* **5**, 17821; doi: 10.1038/srep17821 (2015).



This work is licensed under a Creative Commons Attribution 4.0 International License. The images or other third party material in this article are included in the article's Creative Commons license, unless indicated otherwise in the credit line; if the material is not included under the Creative Commons license, users will need to obtain permission from the license holder to reproduce the material. To view a copy of this license, visit <http://creativecommons.org/licenses/by/4.0/>